Polymorphic transformation of dense ZnO nanoparticles: Implications for chair/boat-type Peierls distortions of AB semiconductor

Chen, Shuei-Yuan; Shen, Pouyan; Jiang, Jianzhong

Published in:
Journal of Chemical Physics

Link to article, DOI:
10.1063/1.1814071

Publication date:
2004

Document Version
Publisher's PDF, also known as Version of record

Polymorphic transformation of dense ZnO nanoparticles: Implications for chair/boat-type Peierls distortions of *AB* semiconductor

Shuei-Yuan Chen[a)]
Department of Mechanical Engineering, I-Shou University, Kaohsiung, Taiwan, Republic of China

Pouyan Shen
Institute of Materials Science and Engineering, National Sun Yat-sen University, Kaohsiung, Taiwan, Republic of China

Jianzhong Jiang
Laboratory of New-Structured Materials, Department of Materials Science and Engineering, Zhejiang University, Hangzhou 310027, People's Republic of China and Department of Physics, Building 307, Technical University of Denmark, Lyngby, Denmark

(Received 13 July 2004; accepted 15 September 2004)

Peierls distortion path was proved experimentally for dense ZnO nanoparticles prepared by static compression. Electron irradiation caused rock salt (R) to wurtzite (W) transition, following preferential $(111)_R//(0\bar{1}11)_W$; $[011]_R//[\bar{1}2\bar{1}3]_W$ and then transformation strain induced $(111)_R//(10\bar{1}1)_W$; $[011]_R//[01\bar{1}1]_W$. The two relationships can be rationalized by specified extent of chair- and boat-type Peierls distortions accompanied with band gap opening and intermediate $\{111\}_R$ slip for energetically favorable $\{111\}_R/(0\bar{1}11)_W$ match. © *2004 American Institute of Physics.* [DOI: 10.1063/1.1814071]

I. INTRODUCTION

Peierls distortions refer to the configurational instabilities associated with a half-filled band of a solid, originally documented for one-dimensional[1] and later two- and three-dimensional structures such as *AB* semiconductor.[2] Upon symmetric structure distortion for coordination number to change, such as from 6 to 4 for rock salt (denoted as R) to wurtzite (denoted as W) transition, the energy gap is opened.[2] While the exact nature of the motion of individual atoms is not well understood, Burdett has shown that much insight can be gained by using symmetry and modeling the $R \rightarrow W$ transition as a Peierls distortion.[3,4] Tolbert and Alivisatos[5] further proposed that such a transition in CdSe nanocrystals may involve so-called "chair-" and "boat" type Peierls distortions by deforming the $\{100\}_R$ into $(0001)_W$ and $\{11\bar{2}0\}$ plane, respectively. This scenario is in accord with acoustic shear modes consideration,[6] although direct experimental evidence for this path yet to be found for analog material such as ZnO focused in this study.

Intrinsic W-ZnO is an n-type semiconductor with a wide direct band gap of 3.37 eV and a high exciton binding energy of 60 meV at ambient pressure[7] for promising applications in the UV region.[8] On the other hand, there is an indirect band gap of 2.45 eV at 13.5 GPa for R-type structure with octahedral coordination[9] originally synthesized at ca. 10 GPa and room temperature.[10] This high-pressure phase in the form of nanosize particles can be retained to ambient pressure due to a sluggish transition[11,12] and therefore suitable for the present *in situ* observations of back transformation, upon electron irradiation at ambient condition, with emphasis on the following points: First, the specific crystallographic relationships of the polymorphs in support of the chair- and boat-type Peierls distortion path, respectively. Second, to rationalize such a lattice correspondence from the standpoint of lattice mismatch. Third, the effect of transformation strain of chair-type on the activation of boat-type distortion as the system goes from finite to bulk.

II. EXPERIMENT

The powdery W-ZnO statically compressed at 15 GPa and 550 K was quenched to ambient condition as R-ZnO particles ca. 12 nm in size according to x-ray diffraction and x-ray absorption spectroscopy.[11] The compact polycrystals were pulverized by an alumina mortar and pestle, and then collected on copper grids overlaid with a carbon-coated collodion film for analytical electron microscopy study using a JEOL 3010 instrument at 300 keV and a beam current of 60 pA/cm^2. Bright field image and selected area electron diffraction (SAED) patterns were used to identify the size distribution and phase identity of the ZnO particles. Lattice imaging coupled with two-dimensional Fourier transform and inverse transform were used to identify the crystallographic relationship defect microstructures due to back transformation of R-ZnO under the effect of electron irradiation at a time interval of 30 s.

III. RESULTS AND DISCUSSION

Transmission electron micrograph (TEM) showed that the pulverized sample consist of randomly oriented particles ca. 10 to 20 nm in size which are predominantly W-ZnO with well-developed $\{10\bar{1}0\}$ surface [Fig. 1(a)]. SAED from

[a)]Author to whom correspondence should be addressed. Fax: +886-7-6578853. Electronic mail: steven@isu.edu.tw

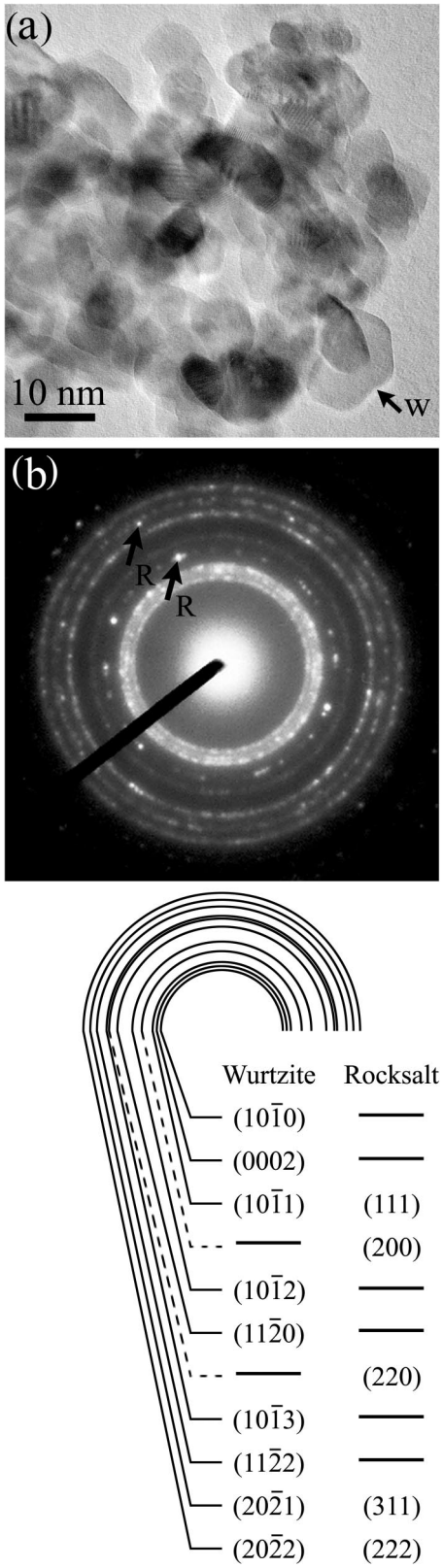

FIG. 1. (a) TEM (bright-field image) of ZnO nanoparticles, predominantly wurtzite structure in hexagonal form (arrow). (b) Ring electron diffractions taken within a selected area aperture of 1 μm. The (200) and (220) diffractions of rock salt structure are indicated by arrows in the pattern and dotted lines in the schematic indexing. Sample statically compressed at 15 GPa and 550 K followed by quenching to ambient condition.

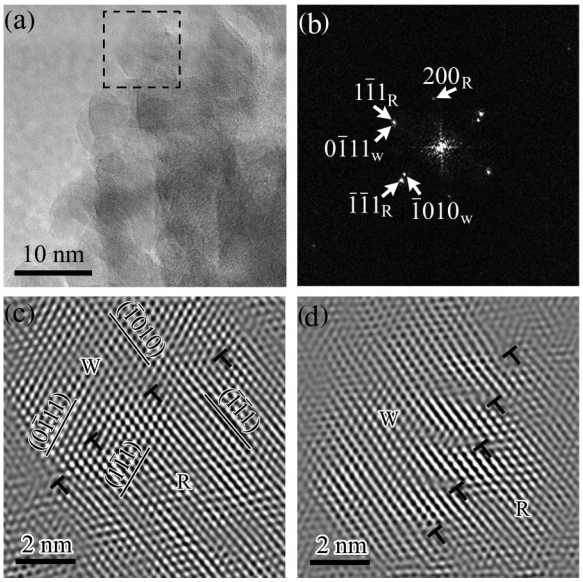

FIG. 2. (a) TEM (lattice image) of ZnO nanoparticles upon electron irradiation for 1 min. (b) Fourier transform and (c) inverse Fourier transform of thin and isolated particle (the square region) in (a) showing the crystallographic relationship $(1\bar{1}1)_R//(0\bar{1}11)_W$; $[011]_R//[\bar{1}2\bar{1}3]_W$ for R-ZnO partially transformed into W-ZnO. (d) The same square region after further irradiation for 1 min causing R/W interface migration toward $(\bar{1}\bar{1}1)_R//(0\bar{1}11)_W$. Note the interfacial dislocations (denoted as T) have a $(\bar{1}\bar{1}1)_R$ half plane.

an area of about 0.8 μm^2 indicated that some particles survived decompression as R-ZnO with characteristic (200) and (220) diffractions [Fig. 1(b)]. These relic particles were used for *in situ* observations of the $R\rightarrow W$ transformation upon electron dosage. An isolated and thin R-ZnO particle [Fig. 2(a)] typically underwent partial transformation into W-ZnO single domain within 1 min of electron irradiation. Fourier transform [Fig. 2(b)] showed the polymorphs followed the crystallographic relationship $(1\bar{1}1)_R//(0\bar{1}11)_W$; $[011]_R//[\bar{1}2\bar{1}3]_W$. The reconstructed image [Fig. 2(c)] further showed that the $\{111\}_R$ planes are either parallel to $(0\bar{1}11)_W$ or $(\bar{1}010)_W$ with a rather rough R/W interface. Dislocation glide on $\{1\bar{1}1\}_R$ planes caused interface migration toward $\sim(1\bar{1}1)_R/(0\bar{1}11)_W$ when irradiated for a total of 2 min [Fig. 2(d)]. The semicoherent interface was decorated with nanometer-spaced edge dislocations having {111} half plane.

As for a typical R-ZnO particle surrounded by yet coalesced particles [Fig. 3(a)], two crystallographic relationships were developed subsequently. The Fourier transform and reconstructed image showed this intact R-ZnO in [011] zone axis [Fig. 3(b)]. Upon electron irradiation for a total of 6 min, two W-domains following $(1\bar{1}1)_R//(0\bar{1}11)_{W1}$; $[011]_R//[\bar{1}2\bar{1}3]_{W1}$, and $(\bar{1}11)_R//(\bar{1}011)_{W2}$; $[011]_R//[0\bar{1}11]_{W2}$ were developed from R-ZnO as indicated by Fourier transform [Fig. 3(c)] and reconstructed image [Fig. 3(d)] [Fig. 3(e)] further showed that the relic R-ZnO has well developed {111} faults before changing into W-structure. The two W-domains adjoined the R-relic with the same type $\{111\}_R/\{0\bar{1}11\}_W$ interface, i.e., $(1\bar{1}1)_R/(0\bar{1}11)_{W1}$ and $(\bar{1}11)_R/(\bar{1}011)_{W2}$. The $\{111\}_R$

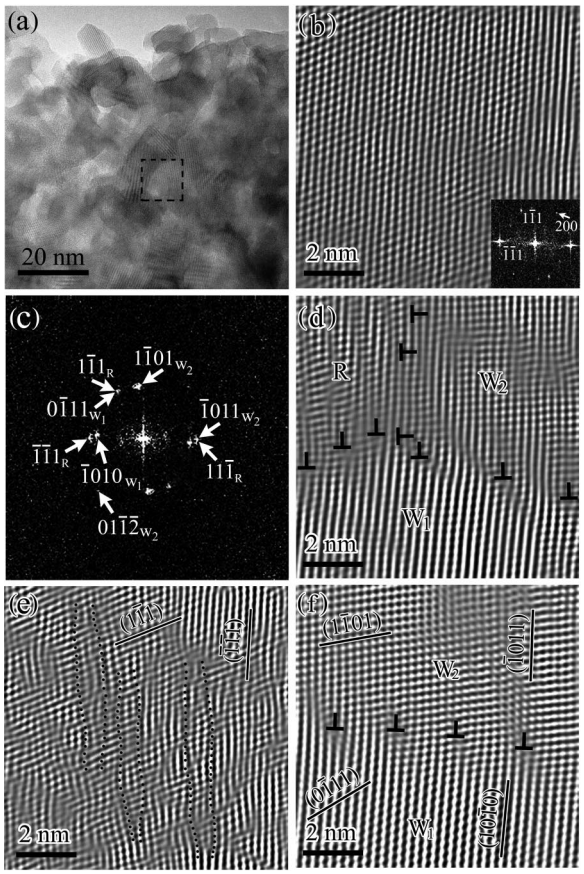

FIG. 3. (a) TEM (lattice image) of ZnO nanoparticles at incipient stage of electron irradiation (ca. 0.5 min) (b) Fourier transform (inset) and inverse Fourier transform of *R*-ZnO ([011] zone axis) surrounded by still coalesced particles, i.e., square region in (a). After electron irradiation for 6 min, Fourier transform (c) and inverse Fourier transform (d) showed two *W*-domains following $(1\bar{1}1)_R//(0\bar{1}11)_{W1}$; $[011]_R//[12\bar{1}3]_{W1}$ and $(\bar{1}11)_R//(10\bar{1}1)_{W2}$; $[011]_R//[01\bar{1}1]_{W2}$. The *R*/*W* interface and W_1/W_2 interface are decorated with interfacial dislocations (*T*). (e) Further left view of relic *R* phase in (d) showing high density of $(\bar{1}11)_R$ fault (dotted lines). (f) Inverse Fourier transform from the square region in (a) after 10 min of electron irradiation showing impinged $[\bar{1}2\bar{1}3]_{W1}$ and $[01\bar{1}\bar{1}]_{W2}$ domains with interfacial dislocations and specifically matched planes labeled (refer to text).

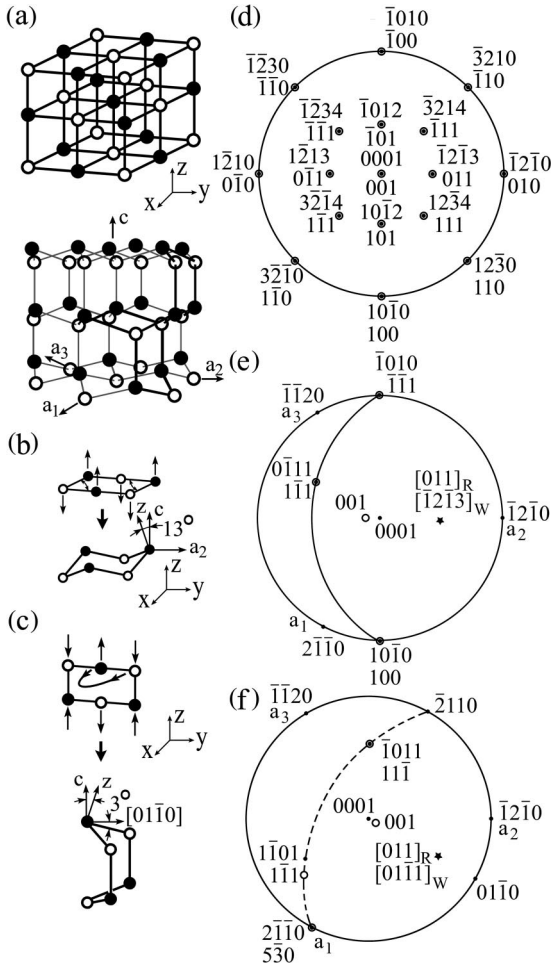

FIG. 4. (a) Rock salt and wurtzite structure with anions and cations denoted by open and solid circles, respectively. One chair-type and two boat-type structures are highlighted in the wurtzite lattice. (b) Schematic drawing showing the middle two atoms of a 2×3 rectangle move apart and the plane puckers to produce a six membered ring chair-type structure in a wurtzite (0001) plane (Ref. 5). Additional 13° tilting along the $(100)_R$ plane is required for the crystallographic relationship specified in (e). (c) In dimension orthogonal to (b), a 2×3 rectangle distorts into wurtzite boat-type structure and additional 3° tilting along the $(2\bar{1}\bar{1}0)_W$ plane as depicted in the $(\bar{1}2\bar{1}0)_W$ projection is essential for the relationship specified in (f). (d), (e), and (f) are corresponding stereograph projections of (a), (b), and (c) constructed with $c/a=1.602$ for *W*-ZnO at ambient pressure (Refs. 14 and 15) (Table I) showing the deviation from ideal case of $(001)_R//(0001)_W$; $(010)_R//(\bar{1}2\bar{1}0)_W$ (d) into (e) and (f) was achieved by tilting $(001)_R$ along the $(100)_R$ and $(2\bar{1}\bar{1}0)_W$, i.e., $(5\bar{3}0)_R$ plane for specified crystallographic relationships. Open and solid circles denote *R* and *W* plane normal, respectively, whereas star denotes direction.

planes are also parallel to $\{0\bar{1}11\}_W$, i.e., $(0\bar{1}11)_{W1}$ and $(10\bar{1}1)_{W2}$ planes, across the interface. The *R*/*W* interface was found to migrate by dislocation (presumably with a Burgers vector of $1/2\langle 110\rangle$ as for analog NaCl structure[13]) gliding on $\{111\}_R$ planes until completion of transformation estimated to be ca. 10 min of electron irradiation. The impinged *W*-domains then have $(10\bar{1}0)_{W1}$ and $(10\bar{1}1)_{W2}$ planes matched despite the migration of the domain boundary [Fig. 3(f) versus Fig. 3(d)].

The lattice correspondence observed in this study indicates deviation from the ideal case of $(001)_R//(0001)_W$; $(010)_R//(\bar{1}2\bar{1}0)_W$ [Fig. 4(a)]. Theoretically, chair-type Peierls distortion is about puckering of $(001)_R$ plane to become $(0001)_W$ plane, i.e., the middle two atoms of a 2×3 rectangle $(001)_R$ plane [Fig. 4(b)] move apart and the plane puckers to produce a six membered ring chair-type structure in a wurtzite (0001) plane [Fig. 4(b)].[5] On the other hand, boat-type Peierls distortion refers to puckering of $(010)_R$ plane to become $(\bar{1}2\bar{1}0)_W$ plane [Fig. 4(c)] or alternatively $(100)_R$ plane to become $(2\bar{1}\bar{1}0)_W$ plane (refer to Fig. 15 of Ref. 5). The observed crystallographic relationships as compiled in the stereograms [Figs. 4(e) and 4(f)] showed that $[001]_R$ originally aligned with $[0001]_w$ became tilted for ca. 13° and 3° along the plane $(100)_R$ and $(2\bar{1}\bar{1}0)_W$, for the chair- and boat-type distortions, respectively. The latter may have a higher activation energy because of two-step puckering of orthogonal $(101)_R$ and $(100)_R$ planes, i.e., apparent tilting of $[001]_R$ along $(5\bar{3}0)_R$ determined by stereographic projection [Fig. 4(f)].

The specific Peierls distortion can be rationalized by

TABLE I. Lattice misfit for hypothetical and observed $(hkl)_R/(hkil)_W$ match. The calculated d spacings of W-ZnO were based on the lattice parameters ($a=0.3250$ nm, $c=0.5207$ nm, space group $P6_3mc$) of synthetic sample at room pressure and temperature (Refs. 14 and 15) and those of R-ZnO were based on the lattice parameter ($a=0.4278$ nm, space group $Fm3m$) measured at room pressure and temperature (Ref. 11). The d spacings of R-ZnO in parenthesis were based on the lattice parameter ($a=0.4128$ nm) measured at 15 GPa (Ref. 16). The hypothetical cases refer to Fig. 4(d) and real cases to Figs. 4(e) and 4(f).

Lattice plane	d spacing (nm)	Misfit (%)	Remark
$12\bar{3}4/111$	0.082/0.247(0.238)	100.3(97.5)	Fig. 4(d)
$1\bar{2}\bar{3}0/110$	0.106/0.303(0.292)	96.3(93.5)	Fig. 4(d)
$\bar{1}\bar{2}10/010$	0.163/0.428(0.413)	89.7(86.8)	Fig. 4(d)
$12\bar{1}3/011$	0.119/0.303(0.292)	87.2(84.2)	Fig. 4(d)
$10\bar{1}2/101$	0.190/0.303(0.292)	45.8(42.3)	Fig. 4(d)
$10\bar{1}0/100$	0.281/0.428(0.413)	41.5(38.0)	Fig. 4(d)
$\bar{0}001/00\bar{1}$	0.521/0.428(0.413)	19.6(21.3)	Fig. 4(d)
$10\bar{1}0/1\bar{1}1$	0.281/0.247(0.238)	12.9(16.6)	Fig. 4(e)
$0\bar{1}11/11\bar{1}$	0.248/0.247(0.238)	0.4(4.1)	Fig. 4(e)
$\bar{1}011/111$	0.248/0.247(0.238)	0.4(4.1)	Fig. 4(f)

anisotropic lattice mismatch strain for the adjoined $(hkl)_R$ and $(hkil)_W$ planes as compiled in Table I, based on x-ray lattice parameters of the polymorphs at various pressures.[11,14–16] The lattice misfit (δ),[17] $\delta=2(d_R-d_W)/(d_R+d_W)$ increases from 0.4% for $\{111\}_R/(0\bar{1}11)_W$, 12.9% for $\{111\}_R/(10\bar{1}0)_W$, and drastically to 19.6% for $(001)_R/(00\bar{0}1)_W$ with accompanied 100% misfit for $\{111\}_R/(12\bar{3}4)_W$ [Fig. 4(d)]. This accounts for the observed two crystallographic relationships both having the $\{111\}_R/\{0\bar{1}11\}_W$ match. By contrast with the boat-type [Fig. 4(f)], the chair-type distortion has additional $\{111\}_R/(10\bar{1}0)_W$ match [Fig. 4(e)]. This indicates that the chair-type distortion path has a larger driving force and indeed preferred to occur in area free of matrix constraint. A significantly smaller d spacing for $\{111\}_R$ than $\{10\bar{1}0\}_W$ (Table I) is also in agreement with extra $\{111\}_R$ half plane for misfit dislocations generated in this Peierls distortion path. The compressive stress associated with a readily activated chair-type distortion during $R\rightarrow W$-ZnO transformation was estimated to be 25.7 GPa given a bulk modulus of 142.6 GPa[9] and volume increase of 18% at ambient pressure.[16] The shear stress due to volume constraint would then trigger boat-type distortion. Under such a case, there are extensive {111} slip and faulting [Fig. 3(e)] as intermediate for further transformation into W-domains.

Distortion of AB semiconductor is about the change of directional bonds and electronic band structure.[3,18] For the present Peierls distortion of R-ZnO prepared at high pressures, the band gap opening at specific pressure is of concern. Given band gap for the polymorphs at specified pressures as mentioned above and the pressure dependence of band gap 24.5 and 25 meV/GPa for W- and R-ZnO, respectively,[9] the band gap opening was calculated to be 1.26 eV at ambient pressure and 1.25 eV at 13.5 GPa. With a significant band gap opening and lattice misfit threshold (Table I), the specific chair- and boat-type Peierls distortion can thus be extended to high pressures at room temperature. The barrier to chair- and boat-type Peierls distortion is a function of the loss of octahedral bonding as the central atoms move apart, balanced against the gain in covalent sp^3 bonds as the system approaches a tetrahedral geometry,[5] with theoretical s electron density increase.[19] Some finite barrier to transition may still exist at the phase transition pressure in view of nonzero shear mode frequency for analogous tetrahedral semiconductors.[5]

Aside from possible ZnO_6 octahedra distortion/rotation upon symmetry/bond breaking to be determined by femtosecond resolution of optical spectroscopy, a lattice-mismatch controlled mechanism of Peierls distortions is established for ZnO semiconductor with ionic character.[20] This transformation mechanism may be valid for other wide-band-gap AB semiconductors at room temperature. The path effects, however, may not be extended to high temperatures where surface diffusion is important.[21]

IV. CONCLUSIONS

We have experimentally characterized the Peierls distortion path for dense ZnO nanoparticles prepared by static compression. Electron irradiation caused back transformation of R structure to W structure, following preferential $(111)_R//(0\bar{1}11)_W$; $[011]_R//[1\bar{2}13]_W$ and then transformation strain induced $(111)_R//(10\bar{1}1)_W$; $[011]_R//[0\bar{1}11]_W$. The two relationships can be rationalized by specified extent of chair- and boat-type Peierls distortions accompanied with band gap opening and intermediate $\{111\}_R$ slip for energetically favorable $\{111\}_R/(0\bar{1}11)_W$ match. The present knowledge of transformation paths for dense ZnO nanoparticles may shed light on chair/boat-type Peierls distortions of AB semiconductor in general.

ACKNOWLEDGMENTS

The authors thank L. J. Wang for her assistance on AEM. Supported by Center for Nanoscience and Nanotechnology at NSYSU, National Science Council of Taiwan, Republic of China under contracts NSC 93-2216-E-214-009, Danish Technical Research Council, and Danish Natural Sciences Research Council. Financial support from the National Natural Science Foundation of China, National Excellent Doctoral Dissertation, and Zhejiang University is gratefully acknowledged.

[1] R. E. Peierls, *Quantum Theory of Solids* (Oxford University Press, London, 1955).
[2] J. K. Burdett and S. Lee, J. Am. Chem. Soc. **105**, 1079 (1983).
[3] J. K. Burdett and T. J. McLarnan, J. Chem. Phys. **75**, 5764 (1981).
[4] J. K. Burdett, Prog. Solid State Chem. **15**, 173 (1984).
[5] S. H. Tolbert and A. P. Alivisatos, J. Chem. Phys. **102**, 4642 (1995).
[6] V. Ozoliņš and A. Zunger, Phys. Rev. Lett. **82**, 767 (1999).
[7] J. M. Hvam, Solid State Commun. **26**, 987 (1978).
[8] N. Kollias, Arch. Dermatol. **135**, 209 (1999).
[9] A. Segura, J. A. Sans, F. J. Manjon, A. Munoz, and M. J. Herrera-Cabera, Appl. Phys. Lett. **83**, 278 (2003), and references cited therein.
[10] C. Bates, W. White, and R. Roy, Science **137**, 993 (1962).
[11] F. Decremps, J. Pellicer-Porres, F. Datchi, J. P. Itie, A. Polin, F. Baudelet, and J. Z. Jiang, Appl. Phys. Lett. **81**, 4820 (2002).

[12] A. Mujica, A. Rubio, A. Munoz, and R. J. Needs, Rev. Mod. Phys. **75**, 863 (2003), and references cited therein.
[13] S. Amelinckx, in *Dislocations in Solids*, edited by F. R. N. Nabarro (North-Holland, Amsterdam, 1979), Vol. 2, p. 381.
[14] S. C. Abrahams and J. L. Bernstein, Acta Crystallogr., Sect. B: Struct. Crystallogr. Cryst. Chem. **25**, 1233 (1969).
[15] B. G. Hyde and S. Andersson, *Inorganic Crystal Structures* (Wiley, New York, 1989).
[16] J. Z. Jiang, J. S. Olsen, L. Gerward, D. Frost, D. Rubie, and J. Peyronneau, Europhys. Lett. **50**, 48 (2000).
[17] J. M. Howe, *Interfaces in Materials* (Wiley, New York, 1997).
[18] D. J. Chadi and R. M. Martin, Solid State Commun. **19**, 643 (1976).
[19] H. Karzel, W. Potzel, M. Köfferlein *et al.*, Phys. Rev. B **53**, 11425 (1996).
[20] F. Decremps, J. Pellicer-Porres, A. M. Saitta, J. C. Chervin, and A. Polian, Phys. Rev. B **65**, 092101 (2002).
[21] S. H. Tolbert and A. P. Alivisatos, Science **265**, 373 (1994).